Weierstraß-Institut
für Angewandte Analysis und Stochastik

Leibniz-Institut im Forschungsverbund Berlin e. V.

Preprint ISSN 2198-5855

Additive manufacturing graded-material design based on phase-field and topology optimization

Massimo Carraturo[1,2], Elisabetta Rocca[3,4], Elena Bonetti[4,5],

Dietmar Hömberg[6,7], Alessandro Reali[1], Ferdinando Auricchio[1]

submitted: November 20, 2018

[1] Dipartimento di Ingegneria
Civile ed Architettura (DICAr)
Universitá degli Studi Pavia
via Ferrata 3
27100 Pavia, Italy
E-Mail: massimo.carraturo01@universitadipavia.it
alessandro.reali@unipv.it
auricchio@unipv.it

[2] Chair for Computation in Engineering
Technical University of Munich
Arcisstr. 21
80333 Munich, Germany

[3] Dipartimento di Matematica
Universitá degli Studi Pavia
via Ferrata 5
27100 Pavia, Italy
E-Mail: elisabetta.rocca@unipv.it

[4] IMATI-CNR
via Ferrata 1
27100 Pavia, Italy

[5] Dipartimento di Matematica “F. Enriques”
Universitá degli Studi di Milano
via Saldini 50
20133 Milano, Italy
E-Mail: elena.bonetti@unimi.it

[6] Weierstrass Institute
Mohrenstr. 39
10117 Berlin, Germany
E-Mail: dietmar.hoemberg@wias-berlin.de

[7] Department of Mathematical Sciences
NTNU
Alfred Getz vei 1
7491 Trondheim, Norway

No. 2553
Berlin 2018

2010 *Mathematics Subject Classification.* 74P05, 49Q10, 35K51.

Key words and phrases. Additive manufacturing, phase-field, multi-material design, topology optimization.

Edited by
Weierstraß-Institut für Angewandte Analysis und Stochastik (WIAS)
Leibniz-Institut im Forschungsverbund Berlin e. V.
Mohrenstraße 39
10117 Berlin
Germany

Fax: +49 30 20372-303
E-Mail: preprint@wias-berlin.de
World Wide Web: http://www.wias-berlin.de/

Additive manufacturing graded-material design based on phase-field and topology optimization

Massimo Carraturo, Elisabetta Rocca, Elena Bonetti,
Dietmar Hömberg, Alessandro Reali, Ferdinando Auricchio

Abstract

In the present work we introduce a novel graded-material design for additive manufacturing based on phase-field and topology optimization. The main novelty of this work comes from the introduction of an additional phase-field variable in the classical single-material phase-field topology optimization algorithm. This new variable is used to grade the material properties in a continuous fashion. Two different numerical examples are discussed, in both of them we perform sensitivity studies to asses the effects of different model parameters onto the resulting structure. From the presented results we can observe that the proposed algorithm adds additional freedom in the design, exploiting the higher flexibility coming from additive manufacturing technology.

1 Introduction

Structural topology optimization [7] is a numerical method which aims, by means of a density function, at optimally distributing a limited amount of material within a volume, representing the initial geometry of a body undergoing specific loads and displacement boundary conditions.

Structural topology optimization was originally introduced as a discrete formulation where areas of dense material and voids are alternated without any transition region [6]. This first approach, also known as *0-1 topology optimization* problem, leads to many difficulties from both an analytical and a numerical point of view [18].

A possible alternative approach is based on homogenization methods, where the macroscopic material properties are obtained from microscopic porous material characteristics [1, 16]. Such a strategy leads to optimized structures with large *grey-scale* regions of perforated, porous material, which are in general undesired due to their elevated manufacturing complexity, in particular when classical manufacturing processes, such as milling or molding are adopted. To obtain a clear *black and white* design, *Solid Isotropic Material Penalization* (SIMP) method has been introduced in [23]. The SIMP method consists of penalizing the density region, different from the void or bulk material, by choosing a suitable interpolation scheme for material properties at the macroscopic scale [5, 8]. This approach has been successfully employed in many engineering applications beside of structural problems, e.g. fluid analysis [14], fluid- and acoustic-structure interaction [21, 22], heat conduction [15], multi-physics [3], and composite structures [19].

An alternative to the SIMP method is a topology optimization based on the phase-field method, for the first time introduced by [11]. Successively, this method has been employed by [12] for stress constrained problems and by [20] in the shape and topology optimization context for minimum compliance and eigenfrequency maximization problems. More recently, [17] have solved nonlinear elastic problems by means of the phase-field approach, while [13] have been the first to apply this method in the context of isogeometric analysis. Similarly to the SIMP method, phase-field based topology optimization penalizes an approximation of the interface perimeter, such that, by choosing a very small positive penalty term, one can obtain a sharp interface region separating solid materials and voids [9].

DOI 10.20347/WIAS.PREPRINT.2553 Berlin 2018

Inspired by the aforementioned works on phase-field-based topology optimization, we aim here at developing an optimization procedure to obtain structures which exploit the possibility of additive manufacturing (AM) technology to distribute material through a body locally varying the material density. Even if such an approach can potentially include a multi-material case, in this work we consider only a graded-material design, i.e., where a single material is gradually distributed through the body. The result of such an optimization routine is a structure with graded stiffness values, i.e., a material with stiffness continuously varying within the body, alternating regions of soft material with other regions of stiffer material. The approach proposed in the present paper reintroduces the typical *grey-scale* regions of early topology optimization methods but within a controlled and numerically stable formulation. This choice is justified by the fact that modern AM technologies allow to grade the density of a body in an almost continuous fashion, varying the amount of distributed material point-by-point during the printing process.

The outline of the work at hand is organized as follows. In Sec. 2 we recall the formulation for a single-material phase-field-based topology optimization. Sec. 3 introduces the novel phase-field approach for graded material structures. Then, Sec. 4 discusses two-dimensional numerical examples, carrying out sensitivity studies for different choices of numerical parameters. Finally, in Sec. 5 we draw our conclusions on the present work.

2 Single-material phase-field topology optimization

In this section we recall the classical formulation for a phase-field-based topology optimization of a single-material homogeneous structure, closely following [10].

2.1 State equations

We consider a domain $\Omega \subset \mathbb{R}^d$ where a material is distributed by means of a scalar phase-field variable ϕ, representing a material density fraction, hence $\phi \in [0,1]$ with $\phi \equiv 0$ corresponding to a void (i.e., no material) and $\phi \equiv 1$ to a dense material. Adopting a linear elastic model, the state equations are as follows:

$$\text{div}\left(\mathbb{C}\boldsymbol{\varepsilon}(\mathbf{u})\right) = \mathbf{0} \quad \text{in} \quad \Omega \tag{1}$$

$$\mathbf{u} = \mathbf{0} \quad \text{on} \quad \Gamma_D \tag{2}$$

$$\mathbb{C}\boldsymbol{\varepsilon}(\mathbf{u}) = \mathbf{g} \quad \text{on} \quad \Gamma_N \tag{3}$$

with $\mathbb{C} = \mathbb{C}(\phi)$ the fourth-order linear material tensor, $\mathbf{u}$ the displacement field vector, $\boldsymbol{\varepsilon}(\mathbf{u})$ the symmetric strain defined as $\boldsymbol{\varepsilon} = \nabla^S \mathbf{u} = \left(\nabla\mathbf{u} + \nabla\mathbf{u}^T\right)/2$, $\mathbf{g}$ the external load on the boundary $\Gamma_N \subset \partial\Omega$, and $\Gamma_D \subset \partial\Omega$, $\mid \Gamma_D \mid \neq 0$, the portion of the boundary where homogeneous Dirichlet boundary conditions are applied.

Assuming the material tensor $\mathbb{C}$ to depend on ϕ, the solution of problem Eq.s (1) to (3) depends on the distribution of the scalar field ϕ (i.e., $\mathbf{u} = \mathbf{u}(\phi)$). We treat the void as a *very soft* material, adopting the following expression for $\mathbb{C}$:

$$\mathbb{C}(\phi) = \mathbb{C}_A \phi^p + \mathbb{C}_B (1-\phi)^p$$

where $\mathbb{C}_A$ is the positive definite material tensor of the dense material, $\mathbb{C}_B$ is the positive definite material tensor of an idealized very soft material (representing the voids), and p can be any positive value; for simplicity, we assume $\mathbb{C}_B = \gamma^2 \mathbb{C}_A$, with $\gamma \ll 1$, while, following [8], we set $p = 3$.

The weak form of the linear elastic problem Eq.s (1) to (3) can be written as:

$$\int_\Omega \boldsymbol{\varepsilon}(\mathbf{u}) : \mathbb{C}(\phi)\boldsymbol{\varepsilon}(\mathbf{v}) \mathrm{d}\Omega = \int_{\Gamma_N} \mathbf{g} \cdot \mathbf{v} \mathrm{d}\Gamma. \tag{4}$$

with $\mathbf{v} \in \mathcal{H}^1_D(\Omega)$ a virtual displacement field. Referring to [10] we can prove that for any given $\mathbf{g} \in L^2(\Gamma_N)$ and $\phi \in L^\infty(\Omega)$, there exists a unique $\mathbf{u} \in H^1_D(\Omega)$ fulfilling Eq. (4) , with $H^1_D(\Omega) := \{\mathbf{v} \in H^1(\Omega) \,:\, \mathbf{v} = \mathbf{0} \quad \text{on } \Gamma_D\}$.

2.2 Single-material topology optimization as a minimization problem

The goal of our topology optimization process is to properly minimize the compliance of a given structure, by optimally distributing a limited amount of material.

To properly minimize the compliance, we introduce an objective functional $\mathcal{J}(\phi, \mathbf{u}(\phi))$ defined as:

$$\mathcal{J}(\phi, \mathbf{u}(\phi)) = \int_{\Gamma_N} \mathbf{g} \cdot \mathbf{u}(\phi) \mathrm{d}\Gamma + \kappa \int_\Omega \left[\frac{\gamma}{2} \parallel \nabla\phi \parallel^2 + \frac{1}{\gamma}\psi_0(\phi) \right] \mathrm{d}\Omega \tag{5}$$

where the first integral represents a measure of the global system compliance, defined as the inverse of the stiffness, while, assuming $\kappa > 0$ and a double-well potential function $\psi_0(\phi) = (\phi - \phi^2)^2$, the second integral is an approximation of the perimeter of the interfaces between regions with $\phi = 0$ and $\phi = 1$. In equation Eq. (5) γ corresponds to the thickness of the diffuse interface, i.e., the region where $0 < \phi < 1$, the term $\gamma/2 \mid \nabla\phi \mid^2$ penalizes jumps between $\phi = 0$ and $\phi = 1$, while $\psi_0(\phi)/\gamma$ represents the double-well potential function penalizing phases with ϕ different from 0 and 1. We remark that following [10] we choose the same scaling parameter γ to penalize the sharp interface region and to define the void soft material; this choice is justified by the assumption that when one of the two values goes to zero also the other one has to vanish.

The minimization of the functional in Eq. (5) is imposed under the assumption of distributing a limited constant quantity of material inside the domain, hence, we introduce the constraint:

$$\int_\Omega \phi \mathrm{d}\Omega = m \mid \Omega \mid$$

with $0 < m \leq 1$ representing a target domain volume fraction. Clearly, the displacement field $\mathbf{u}(\phi)$ solving the topology optimization problem should also be solution of the linear elastic problem of Eq. (4) .

In conclusion, the minimization problem we aim to solve is the following.

Problem $(\mathcal{P})$:

$$\min_\phi \quad \mathcal{J}(\phi, \mathbf{u}(\phi))$$

such that the following constraints are satisfied:

$$\int_\Omega \boldsymbol{\varepsilon}(\mathbf{u}) : \mathbb{C}(\phi)\boldsymbol{\varepsilon}(\mathbf{v}) \mathrm{d}\Omega = \int_{\Gamma_N} \mathbf{g} \cdot \mathbf{v} \mathrm{d}\Gamma. \tag{6}$$

$$\mathcal{M}(\phi) = \int_\Omega \phi \mathrm{d}\Omega - m \mid \Omega \mid = 0, \tag{7}$$

with $\phi \in H^1(\Omega)$ satisfying the constraint:

$$0 \leq \phi \leq 1 \qquad \text{a.e. in } \Omega. \tag{8}$$

Following the argument by [10], we can prove that the minimum constrained problem $(\mathcal{P})$ has at least one solution (cf. [10, Thm. 4.1]). In particular, to solve problem $(\mathcal{P})$ we introduce the Lagrangian functional $\mathcal{L}$, defined as:

$$\mathcal{L}(\phi, \mathbf{u}, \lambda, \mathbf{p}) = \mathcal{J}(\phi, \mathbf{u}) + \lambda\mathcal{M}(\phi) + \mathcal{S}(\phi, \mathbf{u}, \mathbf{p}), \tag{9}$$

where λ is the Lagrange multiplier introduced to impose the volume constrain of Eq. (7) and the operator $\mathcal{S}$ is defined as:

$$\mathcal{S}(\phi, \mathbf{u}, \mathbf{p}) = \int_\Omega \boldsymbol{\varepsilon}(\mathbf{u}) : \mathbb{C}(\phi)\boldsymbol{\varepsilon}(\mathbf{p})\mathrm{d}\Omega - \int_{\Gamma_N} \mathbf{g} \cdot \mathbf{p}\mathrm{d}\Gamma,$$

which we introduce together with the adjoint variable $\mathbf{p}$. The solution of problem $(\mathcal{P})$ is equivalent to the minimization of Eq. (9) subjected to constraint in Eq. (8) ; this last problem problem can be seen as an optimal control problem, with solutions $(\bar{\phi}, \bar{\mathbf{u}}, \bar{\lambda}, \bar{\mathbf{p}})$ that have to satisfy the first order optimality conditions defined by:

$$\begin{aligned} D_{\mathbf{u}}\mathcal{L}\left(\bar{\phi}, \bar{\mathbf{u}}, \bar{\lambda}, \bar{\mathbf{p}}\right) &= 0, \\ D_{\mathbf{p}}\mathcal{L}\left(\bar{\phi}, \bar{\mathbf{u}}, \bar{\lambda}, \bar{\mathbf{p}}\right) &= 0, \\ D_{\lambda}\mathcal{L}\left(\bar{\phi}, \bar{\mathbf{u}}, \bar{\lambda}, \bar{\mathbf{p}}\right) &= 0, \\ D_{\phi}\mathcal{L}\left(\bar{\phi}, \bar{\mathbf{u}}, \bar{\lambda}, \bar{\mathbf{p}}\right)\left(\phi - \bar{\phi}\right) &\geq 0 \qquad\qquad \forall \phi \in \Phi_{ad}, \end{aligned}$$

where Φ_{ad} is the set of admissible controls defined as follows:

$$\Phi_{ad} := \{\phi \in H^1_D(\Omega) \,:\, 0 \leq \phi \leq 1 \quad \text{a.e. in } \Omega\}.$$

We also note that for the problem under investigation $D_{\mathbf{p}}\mathcal{L} = D_{\mathbf{u}}\mathcal{L}$, hence the so-called adjoint equation (holding true for every $\mathbf{v} \in H^1_D(\Omega)$):

$$\int_\Omega \boldsymbol{\varepsilon}(\bar{\mathbf{p}}) : \mathbb{C}(\phi)\boldsymbol{\varepsilon}(\mathbf{v})\mathrm{d}\Omega = \int_{\Gamma_N} \mathbf{g} \cdot \mathbf{v}\mathrm{d}\Gamma,$$

is identical to the weak form of the linear elastic problem Eq. (4) , which implies that $\bar{\mathbf{p}} = \bar{\mathbf{u}}$. We refer to [10] for the complex analysis of optimality conditions.

To obtain a more compact formulation, we define here the energy density of the system and its derivative w.r.t. the scalar field ϕ as:

$$\mathcal{E}(\phi, \mathbf{u}) = \boldsymbol{\varepsilon}(\mathbf{u}) : \mathbb{C}(\phi)\boldsymbol{\varepsilon}(\mathbf{u}),$$

and

$$\frac{\partial \mathcal{E}(\phi, \mathbf{u})}{\partial \phi} = \boldsymbol{\varepsilon}(\mathbf{u}) : \frac{\partial \mathbb{C}(\phi)}{\partial \phi}\boldsymbol{\varepsilon}(\mathbf{u}).$$

To discretize our continuous problem we employ a gradient flow dynamics, namely Allen-Cahn gradient flow [2], a steepest descent pseudo-time stepping method with a time-step increment τ. Thus the optimal control problem $(\mathcal{P})$ can be now rewritten as follows:

$$D_{\mathbf{u}}\mathcal{L}\,\mathbf{v} = 0, \tag{10}$$

$$D_{\lambda}\mathcal{L}\,v_\lambda = \mathcal{M}v_\lambda = 0, \tag{11}$$

$$\frac{\gamma}{\tau}\int_\Omega (\phi_{n+1} - \phi_n)v_\phi \mathbf{dx} = -D_{\phi}\mathcal{L}\,v_\phi, \tag{12}$$

where

$$D_{\phi}\mathcal{L} = \frac{\partial \mathcal{J}}{\partial \phi} + \lambda\frac{\partial \mathcal{M}}{\partial \phi} + \frac{\partial \mathcal{S}}{\partial \phi},$$

with $v_\lambda \in \mathbb{R}$ and $v_\phi \in \Phi_{ad}$.

The problem defined in Eq.s (10) to (12) can be written in the following weak extended formulation:

$$\int_\Omega \boldsymbol{\varepsilon}(\mathbf{u}) : \mathbb{C}(\phi)\boldsymbol{\varepsilon}(\mathbf{v})\mathrm{d}\Omega = \int_{\Gamma_N} \mathbf{g}\cdot\mathbf{v}\mathrm{d}\Gamma, \tag{13}$$

$$\int_\Omega v_\lambda(\phi_{n+1}-m)\mathrm{d}\Omega = 0, \tag{14}$$

$$\begin{aligned}\frac{\gamma}{\tau}\int_\Omega(\phi_{n+1}-\phi_n)v_\phi\mathrm{d}\Omega + \kappa\gamma\int_\Omega \nabla\phi_{n+1}\cdot\nabla v_\phi\mathrm{d}\Omega \\ + \lambda\int_\Omega v_\phi\mathrm{d}\Omega - \int_\Omega v_\phi\frac{\partial\mathcal{E}(\phi_n,\mathbf{u}_n)}{\partial\phi}\mathrm{d}\Omega \\ + \frac{\kappa}{\gamma}\int_\Omega\frac{\partial\psi_0(\phi_n)}{\partial\phi}v_\phi\mathrm{d}\Omega = 0.\end{aligned} \tag{15}$$

2.3 Single-material finite element formulation

We derive here a finite element approximation of the phase-field topology optimization problem defined in Eq.s (13) to (15). To this end we discretize the physical domain Ω using three different meshes $\mathcal{Q}_u$, $\mathcal{Q}_\phi$ and $\mathcal{Q}_\lambda$, corresponding to the field variables $\mathbf{u}$, ϕ and λ and their variations $\mathbf{v}$, v_ϕ and v_λ, respectively. On each mesh we interpolate the nodal values of the field variables and their variations by means of piecewise linear basis functions, such that:

$$\begin{aligned}\mathbf{u} &\approx \mathbf{N}_\mathbf{u}\tilde{\mathbf{u}}, & \mathbf{v} &\approx \mathbf{N}_\mathbf{u}\tilde{\mathbf{v}},\\ \phi &\approx \mathbf{N}_\phi\tilde{\boldsymbol{\phi}}, & v_\phi &\approx \mathbf{N}_\phi\tilde{\mathbf{v}}_\phi,\\ \lambda &\approx \mathbf{N}_\lambda\tilde{\boldsymbol{\lambda}}, & v_\lambda &\approx \mathbf{N}_\lambda\tilde{\mathbf{v}}_\lambda.\end{aligned}$$

Introducing the proposed discretization in Eq.s (13) to (15) the discrete version of the optimal control problem becomes:

$$\begin{aligned}\frac{1}{\tau}\left[\begin{array}{cc|c} \mathbf{0} & \mathbf{0} & \mathbf{0} \\ \mathbf{0} & \mathbf{0} & \mathbf{M}^{\lambda\phi} \\ \hline \mathbf{0} & \mathbf{M}^{\phi\lambda} & \mathbf{M}^{\phi\phi}\end{array}\right]\left[\begin{array}{c}\tilde{\mathbf{u}}\\ \tilde{\boldsymbol{\lambda}}\\ \tilde{\boldsymbol{\phi}}\end{array}\right] + \left[\begin{array}{cc|c} \mathbf{K}^{\mathbf{uu}} & \mathbf{0} & \mathbf{0} \\ \mathbf{0} & \mathbf{0} & \mathbf{0} \\ \hline \mathbf{0} & \mathbf{0} & \mathbf{K}^{\phi\phi}\end{array}\right]\left[\begin{array}{c}\tilde{\mathbf{u}}\\ \tilde{\boldsymbol{\lambda}}\\ \tilde{\boldsymbol{\phi}}\end{array}\right] \\ = \left[\begin{array}{c}\mathbf{f}\\ \mathbf{q}^\lambda\\ \mathbf{q}^\phi+\mathbf{q}^s+\mathbf{q}^\psi\end{array}\right]\end{aligned} \tag{16}$$

with the matrix and vector terms defined as follows:

$$
\begin{aligned}
\mathbf{K}^{\mathbf{uu}} &= \int_{\Omega} \nabla \mathbf{N_u}^T \mathbb{C} \nabla \mathbf{N_u} \mathrm{d}\Omega, \\
\mathbf{M}^{\phi\phi} &= \gamma \int_{\Omega} \mathbf{N}_{\phi}^T \mathbf{N}_{\phi} \mathrm{d}\Omega, \\
\mathbf{K}^{\phi\phi} &= \kappa\gamma \int_{\Omega} \nabla \mathbf{N}_{\phi}^T \nabla \mathbf{N}_{\phi} \mathrm{d}\Omega, \\
\mathbf{M}^{\lambda\phi} &= \tau \int_{\Omega} \mathbf{N}_{\lambda}^T \mathbf{N}_{\phi} \mathrm{d}\Omega = \left(\mathbf{M}^{\phi\lambda}\right)^T, \\
\mathbf{f} &= \int_{\Gamma_N} \mathbf{N_u}^T \mathbf{g} \mathrm{d}\Gamma, \\
\mathbf{q}^{\phi} &= \frac{\gamma}{\tau} \int_{\Omega} \left(\mathbf{N}_{\phi}^T \mathbf{N}_{\phi}\right) \tilde{\boldsymbol{\phi}}_n \mathrm{d}\Omega = \mathbf{M}^{\phi\phi} \tilde{\boldsymbol{\phi}}_n, \\
\mathbf{q}^{\lambda} &= \int_{\Omega} \mathbf{N}_{\lambda}^T m \mathrm{d}\Omega, \\
\mathbf{q}^{s} &= \int_{\Omega} \mathbf{N}_{\phi}^T \frac{\partial \mathcal{E}(\tilde{\boldsymbol{\phi}}_n, \tilde{\mathbf{u}}_n)}{\partial \phi} \mathrm{d}\Omega, \\
\mathbf{q}^{\psi} &= \frac{\kappa}{\gamma} \int_{\Omega} 2\mathbf{N}_{\phi}^T \frac{\partial \psi_0(\tilde{\boldsymbol{\phi}}_n)}{\partial \phi} \mathrm{d}\Omega.
\end{aligned}
$$

The discrete linear system in Eq. (16) can be written in a compact form as:

$$
\left(\frac{1}{\tau}\mathbf{M} + \mathbf{K}\right)\mathbf{x} = \mathbf{q}, \tag{17}
$$

which can be solved with either a direct or an iterative solver. In particular, we solve the problem in Eq. (17) employing Alg. 1 .

Alg. 1 solves the problem in two separate steps: first it solves the state equation discussed in Subsec. 2.1 to get the solution vector $\tilde{\mathbf{u}}_{n+1}$ (line 3), secondly, the remaining system is solved to obtain the phase-field vector $\tilde{\boldsymbol{\phi}^*}_{n+1}$ and the Lagrange multiplier vector $\tilde{\boldsymbol{\lambda}}_{n+1}$ (line 4). The vector $\tilde{\boldsymbol{\phi}^*}_{n+1}$ is then rescaled within the interval $[0, 1]$ to obtain the phase-field solution vector $\tilde{\boldsymbol{\phi}}_{n+1}$ fulfilling the constraints (line 5). We use the increment Δ_{ϕ} based on the L^2-norm and defined as:

$$
\Delta_{\phi} = \frac{\left\| \tilde{\boldsymbol{\phi}}_{n+1} - \tilde{\boldsymbol{\phi}}_n \right\|_{L^2}}{\left\| \tilde{\boldsymbol{\phi}}_n \right\|_{L^2}}, \tag{18}
$$

as a criteria to assert the convergence of the algorithm, which is otherwise stopped when user defined maximum number of iterations max_{iter} is reached.

3 Graded-material phase-field topology optimization

In the following section we extend the previously presented formulation of topology optimization to the case of a graded material definition. We refer to this approach as graded-material phase-field topology optimization. The mathematical analysis of the corresponding optimization problem will be the subject of a forthcoming paper [4].

Algorithm 1: Single-material optimization algorithm

input : $\mathcal{Q}$, $\mathcal{Q}_\phi$, $\mathcal{Q}_\lambda$,$\tilde{\boldsymbol{\phi}}_0$.
output: Optimal topology
$\tilde{\boldsymbol{\phi}}_n \leftarrow \tilde{\boldsymbol{\phi}}_0$
while $\Delta_\phi \geq tol$ *and* $n \leq max_{iter}$ **do**
  $(\tilde{\mathbf{u}}_{n+1}, \tilde{\boldsymbol{\lambda}}_{n+1}, \tilde{\boldsymbol{\phi}}^*_{n+1}) \leftarrow$`solve`(17)
  $\tilde{\boldsymbol{\phi}}_{n+1} \leftarrow$`rescale`$\left(\tilde{\boldsymbol{\phi}}^*_{n+1}\right)$ to $[0,1]$
  `update`(Δ_ϕ)
  $\tilde{\boldsymbol{\phi}}_n \leftarrow \tilde{\boldsymbol{\phi}}_{n+1}$
end

3.1 State equation

We now consider the case of an inhomogeneous material distribution; in particular, we assume that the material elastic fourth-order tensor $\mathbb{C}$ can vary linearly between different positive definite tensors, $\mathbb{C}_A$ and $\mathbb{C}_B$, through a material grading scalar variable $\chi \in [0, \phi]$, with $\phi \in [0, 1]$, such that:

$$\mathbb{C}(\chi) = \mathbb{C}_A\chi + \mathbb{C}_B(\phi - \chi),$$

where the soft material $\mathbb{C}_B$ is defined as:

$$\mathbb{C}_B = \frac{1}{\beta}\mathbb{C}_A,$$

with $0 < \beta \leq 1$ a so-called softening factor, used to define the soft material tensor $\mathbb{C}_B$ as a fraction of the dense material tensor $\mathbb{C}_A$. In such a way, the stiffness of the body can continuously vary from a full dense material ($\chi = \phi$) to a softer one ($\chi = 0$). Therefore, the definition of the fourth-order material tensor $\mathbb{C}(\phi, \chi)$, previously defined in Sec. 2 , can now be modified as:

$$\mathbb{C}(\phi, \chi) = \mathbb{C}(\chi)\phi^p + \gamma_\phi^2\mathbb{C}(\chi)(1 - \phi)^p, \tag{19}$$

where $0 < \gamma_\phi \ll 1$ and again we choose a penalty parameter $p = 3$. The definition of the material tensor in Eq. (19) leads us to an optimized structure where, as in the single-material case, the perimeter of the body is defined by the sharp interface of the phase-field variable ϕ, while the stiffness of the material continuously varies within the structure, following the distribution of the material grading variable χ. Hence, the graded-material weak form of the linear elastic problem of Eq. (4) reads:

$$\int_\Omega \boldsymbol{\varepsilon}(\mathbf{u}) : \mathbb{C}(\phi, \chi)\boldsymbol{\varepsilon}(\mathbf{v})\mathrm{d}\Omega = \int_{\Gamma_N} \mathbf{g} \cdot \mathbf{v}\mathrm{d}\Gamma \tag{20}$$

with the virtual displacement $\mathbf{v} \in H^1_D(\Omega)$.

3.2 Graded-material topology optimization as a minimization problem

We want now to define an objective functional which optimizes a structure with an inhomogeneous material distribution. This new graded-material objective functional $\mathcal{J}^M(\phi, \chi, \mathbf{u}(\phi, \chi))$ can be defined as:

$$\mathcal{J}^M(\phi, \chi, \mathbf{u}(\phi, \chi)) = \int_{\Gamma_N} \mathbf{g} \cdot \mathbf{u}(\phi, \chi)\mathrm{d}\Gamma +$$
$$\kappa_\phi \int_\Omega \left[\frac{\gamma_\phi}{2} \mid \nabla\phi \mid^2 + \frac{1}{\gamma_\phi}\psi_0(\phi)\right] \mathrm{d}\Omega + \kappa_\chi \int_\Omega \frac{\gamma_\chi}{2} \mid \nabla\chi \mid^2 \mathrm{d}\Omega,$$

with $\kappa_\phi, \kappa_\chi > 0$ and $\gamma_\chi > 0$, and where the first two integrals are the same of the objective functional in Eq. (5) , while the additional integral term $\gamma_\chi/2\,(\mid \nabla\chi \mid)^2$ is introduced to penalize the gradient of the scalar field χ.

Following the same approach described for the single-material case, the global graded-material minimization problem can be now written as follows:

$$\begin{aligned}
&\min_{\phi,\chi} \quad \mathcal{J}^M(\phi,\chi,\mathbf{u}(\phi,\chi)),\\
&\int_\Omega \boldsymbol{\varepsilon}(\mathbf{u}) : \mathbb{C}(\phi,\chi)\boldsymbol{\varepsilon}(\mathbf{v})\mathrm{d}\Omega = \int_{\Gamma_N} \mathbf{g}\cdot\mathbf{v}\mathrm{d}\Gamma,\\
&\mathcal{M}(\phi) = \int_\Omega \phi\mathrm{d}\Omega - m \mid \Omega \mid = 0,
\end{aligned}$$

where $\phi, \chi \in H^1(\Omega)$, under the constraint

$$0 \le \phi \le 1 \qquad \text{a.e. in } \Omega,$$

and the additional constraint on χ:

$$0 \le \chi \le \phi \quad \text{a.e. in } \Omega.$$

We can now define the graded-material Lagrangian $\mathcal{L}^M$ as:

$$\begin{aligned}
&\mathcal{L}^M(\phi,\chi,\mathbf{u},\lambda,\mathbf{p}) =\\
&\mathcal{J}^M(\phi,\chi,\mathbf{u}) + \lambda\mathcal{M}(\phi) + \mathcal{S}^M(\phi,\chi,\mathbf{u},\mathbf{p}),
\end{aligned}$$

where, the operator $\mathcal{S}^M$ for the graded-material formulation is calculated as:

$$\mathcal{S}^M(\phi,\chi,\mathbf{u},\mathbf{p}) = \int_\Omega \varepsilon(\mathbf{u}) : \mathbb{C}(\phi,\chi)\varepsilon(\mathbf{p})\mathrm{d}\Omega - \int_{\Gamma_N} \mathbf{g}\cdot\mathbf{p}\mathrm{d}\Gamma.$$

Analogously to the previously introduced set of admissible controls Φ_{ad} for the phase-field variable ϕ, we define now the set of admissible controls Ξ_{ad} for the grading variable χ as:

$$\Xi_{ad} := \{\chi \in H^1(\Omega) \,:\, 0 \le \chi \le \phi \quad \text{a.e. in } \Omega\}.$$

Clearly, also in the graded-material case we want that the optimal control solutions $\bar\phi$ and $\bar\chi$ have to satisfy the first order necessary optimality conditions, which can be derived as:

$$D_\phi\mathcal{L}^M(\bar\phi,\bar\chi,\bar{\mathbf{u}},\bar\lambda,\bar{\mathbf{p}})\left(\phi-\bar\phi\right) \ge 0 \quad \forall\phi\in\Phi_{ad}$$

and

$$D_\chi\mathcal{L}^M\left(\bar\phi,\bar\chi,\bar{\mathbf{u}},\bar\lambda,\bar{\mathbf{p}}\right)(\chi-\bar\chi) \ge 0 \quad \forall\chi\in\Xi_{ad},$$

where $\bar{\mathbf{u}}$ and $\bar{\mathbf{p}}$ are solutions of the graded-material state equation Eq. (20) and of the corresponding adjoint problem, respectively. Also in this case the displacement field $\mathbf{u}$ is self-adjoint and hence we have $\bar{\mathbf{p}} = \bar{\mathbf{u}}$. For a complete analysis of necessary first order optimality conditions we refer to the forthcoming paper [4].

Analogously to the single-material case, we can define the energy density of the system and its derivatives w.r.t. both the scalar field ϕ and the material grading variable χ as:

$$\mathcal{E}^M(\phi,\chi,\mathbf{u}) = \boldsymbol{\varepsilon}(\mathbf{u}) : \mathbb{C}(\phi,\chi)\boldsymbol{\varepsilon}(\mathbf{u}),$$

$$\frac{\partial \mathcal{E}^M(\phi,\chi,\mathbf{u})}{\partial \phi} = \boldsymbol{\varepsilon}(\mathbf{u}) : \frac{\partial \mathbb{C}(\phi,\chi)}{\partial \phi}\boldsymbol{\varepsilon}(\mathbf{u}) =$$
$$\boldsymbol{\varepsilon}(\mathbf{u}) : \left[3\mathbb{C}(\chi)\phi^2 + 3\gamma_\phi^2\mathbb{C}(\chi)(1-\phi)^2\right]\boldsymbol{\varepsilon}(\mathbf{u})$$

and

$$\frac{\partial \mathcal{E}^M(\phi,\chi,\mathbf{u})}{\partial \chi} = \boldsymbol{\varepsilon}(\mathbf{u}) : \frac{\partial \mathbb{C}(\phi,\chi)}{\partial \chi}\boldsymbol{\varepsilon}(\mathbf{u}) =$$
$$\boldsymbol{\varepsilon}(\mathbf{u}) : \left[\left(\mathbb{C}_A - \frac{1}{\beta}\mathbb{C}_A\right)\left(\phi^3 + \gamma_\phi^2(1-\phi)^3\right)\right]\boldsymbol{\varepsilon}(\mathbf{u}).$$

The optimal control problem can be solved as in the single-material case by means of the Allen-Cahn gradient flow, leading to the following set of equations:

$$\frac{\gamma_\phi}{\tau}\int_\Omega (\phi_{n+1}-\phi_n)v_\phi \mathsf{d}\Omega + \kappa_\phi\gamma_\phi\int_\Omega \nabla\phi\cdot\nabla v_\phi \mathsf{d}\Omega + \int_\Omega v_\phi\lambda \mathsf{d}\Omega - \int_\Omega v_\phi \frac{\partial \mathcal{E}^M(\phi_n,\chi_n,\mathbf{u}_n)}{\partial\phi}\,\mathsf{d}\Omega\frac{\kappa_\phi}{\gamma_\phi}\int_\Omega \frac{\partial\psi_0(\phi_n)}{\partial\phi}v_\phi \mathsf{d}\Omega = 0, \quad (21)$$

$$\frac{\gamma_\chi}{\tau}\int_\Omega (\chi_{n+1}-\chi_n)v_\chi \mathsf{d}\Omega + \kappa_\chi\gamma_\chi\int_\Omega \nabla\chi\cdot\nabla v_\chi\,\mathsf{d}\Omega - \int_\Omega v_\chi\frac{\partial \mathcal{E}^M(\phi_n,\chi_n,\mathbf{u}_n)}{\partial\chi}\,\mathsf{d}\Omega = 0, \quad (22)$$

to be solved under the volume constraint

$$\int_\Omega v_\lambda(\phi - m)\mathsf{d}\Omega = 0. \quad (23)$$

In order to estimate the total amount of material in the structure, we define a material fraction index m_χ as:

$$m_\chi = \frac{1}{\mid\Omega\mid}\int_\Omega \chi \mathsf{d}\Omega,$$

which can be considered as a measure of the global amount of material used to print the structure. The equivalent material fraction index for the single-material case m_ϕ is equal to the volume fraction m, such that:

$$m_\phi = m = \frac{1}{\mid\Omega\mid}\int_\Omega \phi \mathsf{d}\Omega.$$

3.3 Graded-material finite element formulation

We aim now at obtaining a discrete formulation for the graded-material phase-field topology optimization problem. To this end, the displacement field $\mathbf{u}$, the phase-field variable ϕ, the Lagrange multiplier λ and their corresponding variations are approximated using the same discretization already defined in Subsec. 2.3 . Additionally, we need to discretize the material grading variable χ on the domain Ω; such a discretization is obtained introducing an additional mesh $\mathcal{Q}_\chi$, such that the material grading variable χ and its variation v_χ can be written as:

$$\chi \approx \mathbf{N}_\chi\tilde{\boldsymbol{\chi}} \qquad \text{and} \qquad v_\chi \approx \mathbf{N}_{v_\chi}\tilde{\mathbf{v}}_\chi,$$

where $\mathbf{N}_\chi$ and $\mathbf{N}_{v_\chi}$ are the piecewise linear shape functions which interpolate the nodal degrees of freedoms $\tilde{\boldsymbol{\chi}}$ and $\tilde{\mathbf{v}}_\chi$, respectively.

The discrete form of Eq.s (21) to (23) can thus be written in a compact notation as:

$$\frac{1}{\tau}\begin{bmatrix}\mathbf{0} & \mathbf{0} & \mathbf{0} & \mathbf{0}\\ \mathbf{0} & \mathbf{M}^{\phi\phi} & \mathbf{0} & \mathbf{M}^{\phi\lambda}\\ \mathbf{0} & \mathbf{0} & \mathbf{M}^{\chi\chi} & \mathbf{0}\\ \mathbf{0} & \mathbf{M}^{\lambda\phi} & \mathbf{0} & \mathbf{0}\end{bmatrix}\begin{bmatrix}\tilde{\mathbf{u}}\\ \tilde{\boldsymbol{\phi}}\\ \tilde{\boldsymbol{\chi}}\\ \tilde{\boldsymbol{\lambda}}\end{bmatrix}+\begin{bmatrix}\mathbf{K}^{\mathbf{uu}} & \mathbf{0} & \mathbf{0} & \mathbf{0}\\ \mathbf{0} & \mathbf{K}^{\phi\phi} & \mathbf{0} & \mathbf{0}\\ \mathbf{0} & \mathbf{0} & \mathbf{K}^{\chi\chi} & \mathbf{0}\\ \mathbf{0} & \mathbf{0} & \mathbf{0} & \mathbf{0}\end{bmatrix}\begin{bmatrix}\tilde{\mathbf{u}}\\ \tilde{\boldsymbol{\phi}}\\ \tilde{\boldsymbol{\chi}}\\ \tilde{\boldsymbol{\lambda}}\end{bmatrix}= \begin{bmatrix}\mathbf{f}\\ \mathbf{q}^{\phi}+\mathbf{q}^{s\prime}+\mathbf{q}^{\psi}\\ \mathbf{q}^{\chi}+\mathbf{q}^{t}\\ \mathbf{q}^{\lambda}\end{bmatrix} \tag{24}$$

where the newly defined matrix and vector terms are:

$$\begin{aligned}\mathbf{M}^{\chi\chi} &= \gamma_{\chi}\int_{\Omega}\mathbf{N}_{\chi}^{T}\mathbf{N}_{\chi}\mathrm{d}\Omega,\\ \mathbf{K}^{\chi\chi} &= \kappa_{\chi}\gamma_{\chi}\int_{\Omega}\nabla\mathbf{N}_{\chi}^{T}\nabla\mathbf{N}_{\chi}\mathrm{d}\Omega,\\ \mathbf{q}^{\chi} &= \frac{\gamma_{\chi}}{\tau}\int_{\Omega}\mathbf{N}_{\chi}^{T}\mathbf{N}_{\chi}\tilde{\boldsymbol{\chi}}_{n}\mathrm{d}\Omega,\\ \mathbf{q}^{s\prime} &= \int_{\Omega}\mathbf{N}_{\phi}^{T}\frac{\partial\mathcal{E}^{M}(\tilde{\boldsymbol{\phi}}_{n},\tilde{\boldsymbol{\chi}}_{n},\tilde{\mathbf{u}}_{n})}{\partial\chi}\mathrm{d}\Omega,\\ \mathbf{q}^{t} &= \int_{\Omega}\mathbf{N}_{\phi}^{T}\frac{\partial\psi_{0}(\tilde{\boldsymbol{\phi}}_{n})}{\partial\phi}\mathrm{d}\Omega.\end{aligned}$$

Alg. 2 describes the iterative procedure to obtain the graded-material optimized structure discussed so far. The adopted solution scheme is very similar to Alg. 1 but in this case we have to solve at each iteration the graded-material linear system defined in Eq. (24) to obtain the phase-field solution vector $\tilde{\boldsymbol{\phi}}_{n+1}$ and the grading scalar variable vector $\tilde{\boldsymbol{\chi}}_{n+1}$.

Algorithm 2: Graded-material optimization algorithm

input : $\mathcal{Q}$, $\mathcal{Q}_{\phi}$, $\mathcal{Q}_{\chi}$, $\mathcal{Q}_{\lambda}$, $\boldsymbol{\phi}_0$, $\boldsymbol{\chi}_0$

. **output:** Optimal topology

$\boldsymbol{\phi}_n \leftarrow \boldsymbol{\phi}_0$

$\boldsymbol{\chi}_n \leftarrow \boldsymbol{\chi}_0$

while $\Delta_{\phi} \geq tol$ *and* $n \leq max_{iter}$ **do**

  $(\tilde{\mathbf{u}}_{n+1}, \tilde{\boldsymbol{\phi}}^{*}_{n+1}, \tilde{\boldsymbol{\chi}}^{*}_{n+1}, \tilde{\boldsymbol{\lambda}}_{n+1}) \leftarrow$ `solve`(24)

  $\tilde{\boldsymbol{\phi}}_{n+1} \leftarrow$ `rescale` $\left(\tilde{\boldsymbol{\phi}}^{*}_{n+1}\right)$ to $[0,1]$

  $\tilde{\boldsymbol{\chi}}_{n+1} \leftarrow$ `rescale` $\left(\tilde{\boldsymbol{\chi}}^{*}_{n+1}\right)$ to $[0,\phi]$

  `update`(Δ_{ϕ})

  $\boldsymbol{\phi}_n \leftarrow \boldsymbol{\phi}_{n+1}$

  $\boldsymbol{\chi}_n \leftarrow \boldsymbol{\chi}_{n+1}$

end

4 Numerical Examples

In this section two numerical examples are presented: in the first one we consider a cantilever beam structure while in the second one we study a simply-supported beam structure. In the cantilever beam

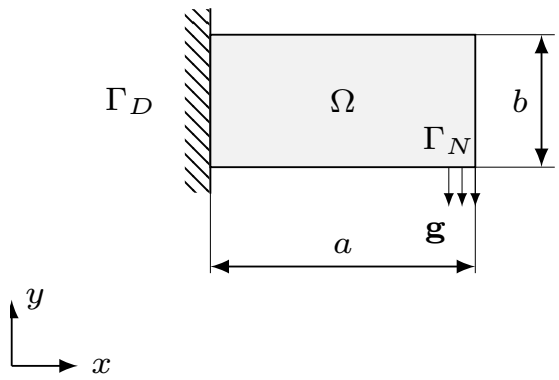

Figure 1: Cantilever beam: Initial configuration and problem domain.

example we discuss two sensitivity studies. Firstly, we vary the values of the graded-material interface parameter γ_χ (i.e., the parameter which represents the thickness of the material grading variable interface) and, secondly, we change the slenderness of the structure. In the simply-supported beam example, again we perform two studies. In the first one we use different values for the softening factor β while in the second one we increase the load acting on the structure.

4.1 Cantilever beam

We consider the cantilever beam problem depicted in Fig. 1 , with dimensions $a = 2$mm and $b = 1$mm and a traction force $\mathbf{g} = (0, -600)$N/mm applied at the right-end of the lower edge of the structure, while the left edge is fixed. We assume the initial material being a dense isotropic material, i.e., $\mathbb{C}_A = (\lambda + 2\mu)\mathbf{1} \otimes \mathbf{1} + 2\mu\mathbf{I}$, where the Lame's parameters λ and μ can be expressed in terms of the Young modulus E and the Poisson coefficient ν as follows:

$$\lambda = \frac{E}{(1+\nu)(1-2\nu)}, \tag{25}$$

and

$$\mu = \frac{E}{2(1+\nu)}. \tag{26}$$

The softening factor β is chosen equal to 4, i.e., the soft material tensor $\mathbb{C}_B$ is four times softer than $\mathbb{C}_A$. We choose a dense material having $E = 12.5$GPa and $\nu = 0.25$. We discretize the domain Ω using a mesh with 128×64 quadrilateral elements and we set $m = 0.45$, $\kappa_\chi = \kappa_\phi = 4$, $\gamma_\phi = 0.02$, a time step increment $\Delta\tau = 1.0 \times 10^{-6}$, $\phi_0 = 0.5$ as initial solution, and a tolerance equal to 0.01.

4.1.1 Sensitivity study of the graded-material interface parameters γ_χ

In this first sensitivity study we investigate the different topologies obtained by varying γ_χ between 0.001 and 0.1, as reported in Fig. 2 . The results show that the optimal multi-material distribution is very different from the single-material optimized topology depicted in Fig. 3 , for values of γ_χ smaller than γ_ϕ. In fact, in this case, the voids present in the single-material structure are replaced by areas of soft material. Contrary, if γ_χ is chosen to be bigger than γ_ϕ the solution presents void regions similarly to the single-material case. Finally, we observe that, as expected, when the thickness of the diffuse interface is too small compared to the element size, the solution does not converge anymore (Fig. 2a). Table 1 reports the values of the compliance and of the material fraction index m_χ for different values of γ_χ. It can be seen that employing a softer material will increase the compliance of the body, leading at the same time to lighter structures compared to the homogeneous material case.

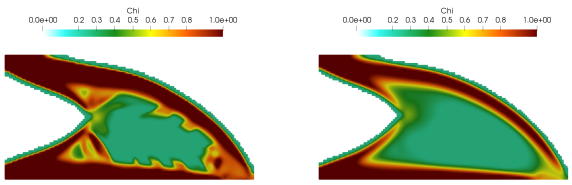

(a) $\gamma_\chi = 0.001$ (b) $\gamma_\chi = 0.005$

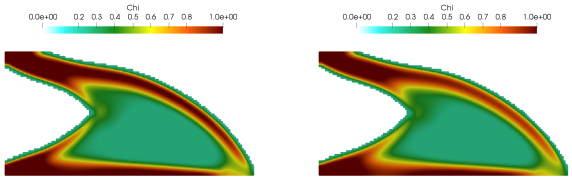

(c) $\gamma_\chi = 0.010$ (d) $\gamma_\chi = 0.020$

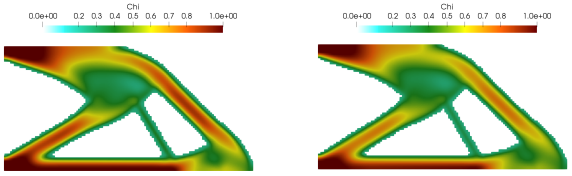

(e) $\gamma_\chi = 0.050$ (f) $\gamma_\chi = 0.100$

Figure 2: Cantilever beam: Sensitivity study of the multi-material interface parameters γ_χ. If $\gamma_\chi \leq \gamma_\phi = 0.02$ different values of the graded-material interface parameters do not affect too much the final solution, which presents a wide region of soft material filling the voids which, instead, characterize the single-material solution (see Fig. 3); whereas, for $\gamma_\chi \geq \gamma_\phi$, the final solution of the graded-material case tends to a single-material configuration with multiple holes in the structure. Finally, if we choose γ_χ too small with respect to our element size, the solution do not converge anymore as in Fig. 2a .

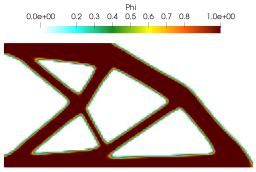

Figure 3: Cantilever beam: Sensitivity study of the graded-material interface parameters γ_χ. Single-material optimized structure.

4.1.2 Sensitivity study of the slenderness of the structure

On the cantilever beam we perform a second sensitivity study varying the slenderness ratio $s = a/b$ (i.e., the ratio between the length and the height of the cantilever beam), for a fixed value of the graded-material interface parameter ($\gamma_\chi = 0.02$). Fig. 4 shows the final topologies for three different slenderness ratios, where all the resulting structures are characterized by internal regions of softer material and an external support of stiffer material.

Table 1: Cantilever beam: Sensitivity study of the graded-material interface parameters γ_χ. Compliance and material index values for different choices of γ_χ.

γ_χ	compliance	m_χ	convergence
0.001	105.3	0.380	NO
0.005	122.9	0.265	YES
0.01	133.0	0.245	YES
0.02	141.9	0.230	YES
0.05	154.0	0.225	YES
0.1	165.4	0.201	YES
full dense material	52.3	$m_\phi = 0.45$	YES

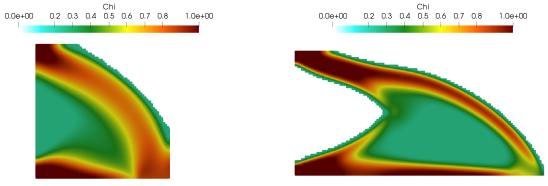

(a) $s = 1$ (b) $s = 2$

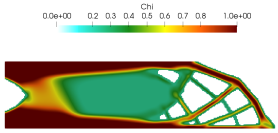

(c) $s = 4$

Figure 4: Cantilever beam: Sensitivity study of the slanderness of the structure s. Varying the slanderness ratio $s = a/b$ we obtain optimized structures characterized by an outer frame of stiff material filled with regions of soft materials.

4.2 Simply-supported beam

In this second example we choose Acrylonitrile Butadiene Styrene (ABS), which is a common thermoplastic polymer widely used in 3D-printing applications, as material to obtain an optimized simply-supported beam structure. The problem is symmetric and thus we decide to solve only half of the domain as depicted in Fig. 5 , where $h = 1$mm an $L/2 = 2$mm, with a distributed external load g equal to $(0, -50)$N/mm applied on the top edge of the structure. The Young modulus and the Poisson coefficient of ABS plastic are 2.3GPa and 0.35, respectively. We set $m = 0.4$, $\kappa_\phi = \kappa_\chi = 1$ and $\gamma_\phi = \gamma_\chi = 0.01$, while we choose a pseudo-time step $\Delta\tau = 1.0 \times 10^{-6}$ and an initial solution $\phi_0 = 0.5$.

4.2.1 Sensitivity study of the softening factor β

Fig. 6 presents the results of a sensitivity analysis performed varying the softening factor β from 1 to 4. The resulting optimized structures show that, introducing *grey-scale* regions in the structure, the optimal design is modified, replacing the typical voids of SIMP approach with areas of soft material. Again we observe in Table 2 that introducing a soft material within the algorithm leads to structure with

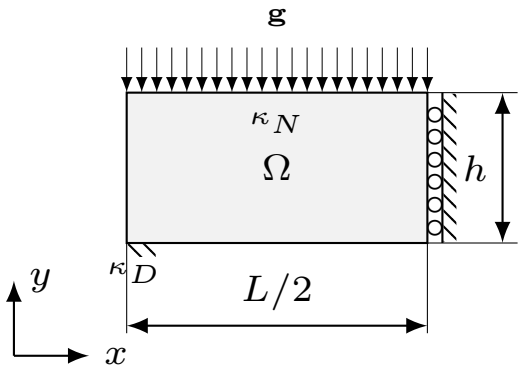

Figure 5: Simply-supported beam: Initial configuration and problem domain.

Table 2: Simply-supported beam: Sensitivity study of the softening factor β. Compliance and material index values for different choices of β.

β	compliance	m_χ	convergence
1	20.5	0.40	YES
2	37.3	0.32	YES
3	46.4	0.24	YES
4	58.6	0.18	YES

a smaller material index but a lower compliance. The values of the softening factor strongly influences the final results and give us the possibility to obtain intermediate structure such as the one in Fig. 6b .

4.2.2 Sensitivity study of the distributed load

On the simply-supported beam we conduct a second sensitivity study fixing $\beta = 3$ and increasing the distributed load g by a factor of 2 and 3, respectively. The resulting structures are reported in Fig. 7 . As we expected employing a heavier load reduces the areas of soft material, increasing at the same time the number of columnar structures in the final topology. We want to remark here that the structure of Fig. 7b did not converge even after 1000 iterations. Since the mesh is not modified, this behavior is due to the choice of the stiffer material, which is in this case too soft for such a heavy load.

5 Conclusions

In the present work we have introduced a novel phase-field topology optimization algorithm based on a graded material definition.

The numerical results show that the additional control parameter χ, introduced in our phase-field formulation, allows to increase the number of possible optimal designs delivered by the topology optimization process.

In particular, we have introduced the possibility to control the distribution of the material density within our structure in a continuous fashion. Such a feature can be in many cases highly desirable, in particular if we consider additive manufacturing applications.

Moreover the algorithm allows to easily control the amount of regions with graded material distribution,

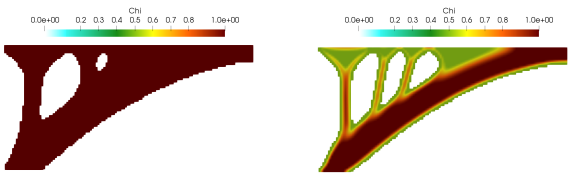

(a) $\beta = 1$ (b) $\beta = 2$

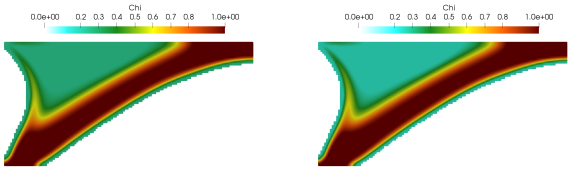

(c) $\beta = 3$ (d) $\beta = 4$

Figure 6: Simply-supported beam: Sensitivity study of the softening factor β. Increasing the values of the softening factor, i.e., employing a softer material, the optimized structure does not present anymore the typical holes resulting from a single-material optimization 6a. Voids are now replaced by a region of soft material.

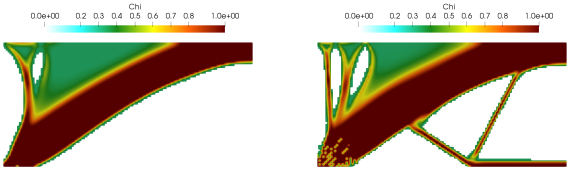

(a) $\mathbf{g} \times 2$ (b) $\mathbf{g} \times 3$

Figure 7: Simply-supported beam: Sensitivity study of the distributed load $\mathbf{g}$. Increasing the load on the upper edge of the structure we observe an increment in the region occupied by full dense material and the presence of holes and columnar structures.

delivering results which can be in between a fully *black-and-white* approach and a purely graded-material distribution.

In the near future we aim at investigating mechanical properties of 3D-printed structures designed using the graded-material phase-field topology optimization algorithm.

Acknowledgements. This work was partially supported by Regione Lombardia through the project "TPro.SL - Tech Profiles for Smart Living"(No. 379384) within the Smart Living program, and through the project "MADE4LO - Metal ADditivE for LOmbardy"(No. 240963) within the POR FESR 2014-2020 program. MC and AR have been partially supported by Fondazione Cariplo - Regione Lombardia through the project “Verso nuovi strumenti di simulazione super veloci ed accurati basati sull’analisi isogeometrica”, within the program RST - rafforzamento. This research has been performed in the framework of the project Fondazione Cariplo-Regione Lombardia MEGAsTAR “Matematica d’Eccellenza in biologia ed ingegneria come acceleratore di una nuova strateGia per l’ATtRattività dell’ateneo pavese”. The present paper also benefits from the support of the GNAMPA (Gruppo Nazionale per l’Analisi Matematica, la Probabilità e le loro Applicazioni) of INdAM (Istituto Nazionale di Alta Matematica) for ER.

References

[1] G. Allaire, F. Jouve, and H. Maillot. Topology optimization and optimal shape design using homogenization. *Struct. Multidisc. Optim.*, 28:87–98, 2004.

[2] S. M. Allen and J. W. Cahn. A microscopic theory for antiphase boundary motion and its application to antiphase domain coarsening. *Acta Metallurgica*, 27(6):1085–1095, June 1979.

[3] C. S. Andreasen and O. Sigmund. Topology optimization of fluid-structure-interaction problems in poroelasticity. *Comput. Methods Appl. Mech. Engrg.*, 31(4):55–62, 2013.

[4] F. Auricchio, E. Bonetti, M. Carraturo, D. Hömberg, A. Reali, and E. Rocca. Structural multiscale topology optimization with stress constraint for additive manufacturing. *Work in progress*, 2018.

[5] M. Bendsøe and O. Sigmund. *Topology Optimization - Theory, Methods, and Applications*. Springer Verlag, Germany, 2003.

[6] M. P. Bendsøe. On obtaining a solution to optimization problems for solid, elastic plates by restriction of the design space. *J. Struct. Mech.*, 11(4):501–521, 1983.

[7] M. P. Bendsøe and N. Kikuchi. Generating optimal topologies in structural design using a homogenization method. *Comput. Methods Appl. Mech. Engrg.*, 71:197–224, 1988.

[8] M. P. Bendsøe and O. Sigmund. Material interpolation schemes in topology optimization. *Archive of Applied Mechanics 6*, 65:635–654, 1999.

[9] L. Blank, M. H. Farshbaf-Shaker, H. Garcke, C. Rupprecht, and V. Styles. Multi-material Phase Field Approach to Structural Topology Optimization. In G. Leugering, P. Benner, S. Engell, A. Griewank, H. Harbrecht, M. Hinze, R. Rannacher, and S. Ulbrich, editors, *Trends in PDE Constrained Optimization*, volume 165, pages 231–246. Springer International Publishing, Cham, 2014.

[10] L. Blank, H. Garcke, M. Farshbaf-Shaker, and V. Styles. Relating phase field and sharp interface approaches to structural topology optimization. *ESAIM Control Optim. Calc. Var.*, 20:1025–1058, 2014.

[11] B. Bourdin and A. Chambolle. Design-dependent loads in topology optimization. *ESAIM Contr. Optim.Calc. Var.*, 9:19–48, 2003.

[12] M. Burger and R. Stainko. Phase-field relaxation of topology optimization with local stress constraints. *SIAM Journal on Control and Optimization*, 45(4):1447–1466, 2006.

[13] L. Dedè, M. J. Borden, and T. J. Hughes. Isogeometric analysis for topology optimization with a phase field model. *Archives of Computational Methods in Engineering*, 19(3):427–465, 2012.

[14] A. Gersborg-Hansen, M. P. Bendsøe, and O. Sigmund. Topology optimization of channel flow problems. *Struct. Multidiscip. O.*, 30(3):181–192, 2005.

[15] A. Gersborg-Hansen, M. P. Bendsøe, and O. Sigmund. Topology optimization of heat conduction using the finite volume method. *Struct. Multidiscip. O.*, 31(4):251–259, 2006.

[16] S. K and N. Kikuchi. A homogenization method for shape and topology optimization. *Comput. Methods Appl. Mech. Engrg.*, 93(3):291–318, 1991.

[17] P. Penzler, M. Rumpf, and B. Wirth. A phase-field model and minimal compliance shape optimization in nonlinear elasticity. *ESAIM Control Optim. Calc. Var.*, 2012:229–258, 2012.

[18] O. Sigmund and J. Petersson. Numerical instabilities in topology optimization: A survey on procedures dealing with cheackboards, mesh-dependencies and local minima. *Structural Optimization*, 16:68–75, 1998.

[19] O. Sigmund and S. Torquato. Composites with extremal thermal expansion coefficients. *Appl. Phys. Lett.*, 69(21):3203–3205, 1996.

[20] A. Takezawa, S. Nishiwaki, and M. Kitamura. Shape and topology optimization based on the phase field method and sensitivity analysis. *J. Comp. Phys.*, 229(7):2697–2718, 2010.

[21] G. H. Yoon. Topology optimization for stationary fluid-structure interaction problems using a new monolithic formulation. *Int. J. Numer. Methods Engrg.*, 82(5):591–616, 2010.

[22] G. H. Yoon, J. Jensen, and S. O. Topology optimization of acoustic–structure interaction problems using a mixed finite element formulation. *Int. J. Numer. Methods Engrg.*, 70(9):1049–1075, 2007.

[23] M. Zhou and G. I. N. Rozvany. The coc algorithm, part ii: Topological geometry and generalized shape optimization. *Comp. Meth. Appl. Mech. Engng.*, 89:197–224, 1991.